JOURNAL OF AIRCRAFT
Vol. 46, No. 5, September–October 2009

Investigation of Unswept Normal Shock Wave/ Turbulent-Boundary-Layer Interaction Control

Jonathan S. Couldrick,* Sudhir L. Gai,† John F. Milthorpe,‡ and Krishna Shankar§
University of New South Wales, Australian Defence Force Academy, Canberra, Australian Capital Territory 2600, Australia

DOI: 10.2514/1.42104

An analytical model for the unswept normal shock wave/turbulent-boundary-layer interaction control using an upstream and downstream unimorph piezoelectric flap actuator has been proposed. The amount of flap deflection controls the bleed/suction rate through a plenum chamber. The cavity allows rapid thickening of the boundary layer approaching a normal shock wave, which splits into a series of weaker shocks forming a lambda shock foot, leading to a reduction in the wave drag. The analysis provides an understanding of the control influences produced in an experimental investigation of an unswept normal shock wave/turbulent-boundary-layer interaction at a Mach number of 1.5. It has also been validated by application to the normal shock wave/boundary-layer interaction control system using mesoflaps for aeroelastic transpiration described in previous transonic/supersonic shock wave/ boundary-layer interaction studies.

I. Introduction

THE interaction of a shock wave with a boundary layer is a classic viscous/inviscid interaction problem that occurs over a wide range of high-speed aerodynamic flows, such as on transonic wings, in supersonic air intakes, at control surface deflections, and propelling nozzles at off-design conditions, just to name a few. On an aerofoil in transonic flow, for instance, when the nearly normal shock wave interacts with a boundary layer, phenomena ranging from a mild increase in section drag to flow separation, eventually leading to buffeting, can occur, depending on the strength of the shock and the state of the boundary layer.

Herein, we address the problem of controlling the interaction of a normal shock wave with a turbulent boundary layer such as that which occurs on the rear of a transonic aerofoil. However, the approach is equally applicable to the control of any interaction wherein the shock wave, either normal or oblique, meets with a turbulent boundary layer.

In view of the adverse effects, such as flow separation and drag increase as a consequence of shock wave/boundary-layer interaction, a number of methods have been explored to control the interaction. However, in general, they have not been very successful, mainly because the drag reduction achieved has been negated by the attendant increase in power expended in removing or energizing, for example, the boundary-layer mass by suction or injection, or, in the case of vortex generators, drag created by their addition alone.

Passive control of the interaction, wherein the boundary layer on a porous surface covering a plenum chamber, as shown in Fig. 1, is interacting with a shock, has shown that considerable wave drag reductions can be achieved in principle. However, in most instances, the skin friction component of the drag over a porous (rough) surface is unacceptable and the overall drag reduction becomes insignificant. Secondly, passive control may result in an increase in skin friction drag in the absence of a shock or when the shock location is outside of the control region as can happen at off-design conditions. Then, there is also the constraint that it is not easily possible to switch on or off the passive control technique. Passive techniques of shock wave/ boundary-layer interaction (SBLI) control have been analyzed and studied for many years, for example, see Nagamatsu et al. [1], Raghunathan [2], Gibson et al. [3], and Delery and Bur [4].

In recent years, a novel method of passive control of SBLI using mesoflaps has been proposed by the researchers at the University of Illinois at Urbana–Champaign [5–7]. In this method, termed mesoflaps for aeroelastic transpiration (MART), an array of aeroelastically tailored flaps are placed underneath the shock foot covering the recirculation cavity. The flaps remain closed in the absence of the shock but deflect due to pressure difference across when a shock wave is present, thereby creating a flow circulation that controls the shock. In particular, the flaps downstream of the shock deflect down due to the pressure increase downstream of the shock. Upstream of the shock, the flaps deflect upward as a consequence of the pressures being lower than in the cavity. The flow circulation across the shock so set up energizes the low-momentum upstream boundary layer and spreads the shock foot, thus avoiding flow separation and increase in viscous and wave drag. Thus, the advantage of such flaps is that, not only is there no increase in the drag in the absence of the shock, because with the flaps closed, the surface is smooth and behaves as a solid wall, but also the bleed flow is nearly *tangential* both upstream and downstream of the shock, leading to smaller losses.

The present paper reports an investigation of an SBLI control system, which can be considered a variant of the MART system. In this system, piezoelectrically controlled flap actuators are used to control the SBLI. The actuators are designed using PZT-5H piezoelectric material to control bleed/suction rate. The flaps are made up of unimorph construction wherein the piezoelectric ceramic is bonded to an inert substrate and applying an electric field to the piezoelectric ceramic will induce deflection [8–11]. The flaps would thus deflect, firstly, due to pressure difference created by the pressure rise across the shock, and secondly, due to piezoelectrically induced strains. In this respect, the flaps can be considered smart and the control "active" in a broad sense because they can be activated to control the recirculation rate or can be switched off, leaving the recirculation rate uncontrolled. The piezoelectric material was selected for flap construction due to its bipolar nature, which is the ability to produce positive or negative strain. This bipolar characteristic enables it to assist the flap's aeroelastic deflection up or down to control the mass transfer. Full details of structural analysis of unimorph flap actuators and the evaluation of their performance is given in [2,11]. Figure 2 illustrates the schematic arrangement of the system.

Presented as Paper 3198 at the Third AIAA Flow Control Conference, San Francisco, CA, 5–8 June 2006; received 10 November 2008; accepted for publication 17 May 2009.

*Student, School of Aerospace, Civil and Mechanical Engineering.
†Visiting Senior Research Fellow, School of Aerospace, Civil and Mechanical Engineering. Associate Fellow AIAA.
‡Visiting Fellow, School of Aerospace, Civil and Mechanical Engineering. Senior Member AIAA.
§Senior Lecturer, School of Aerospace, Civil and Mechanical Engineering.

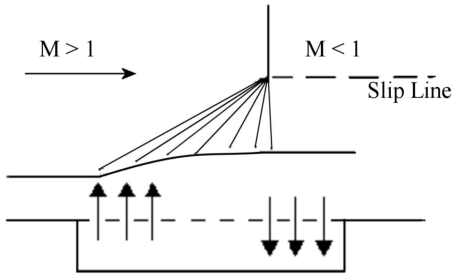

Fig. 1 Passive control of the shock wave /boundary-layer interaction.

In what follows, we present an analysis of the normal shock/boundary-layer interaction flow and a plenum with flap actuators. We then apply the results of the analysis to the MART system of normal SBLI control [5] and then finally validate the results with our own experimental data.

II. Theoretical Considerations

A. Analytical Model

Although, in practice, the upstream flap deflects upward, and the downstream one deflects downward, as shown in Fig. 2, in our modeling, we assume that the downstream flap will not deflect but an equivalent orifice flow into the plenum chamber occurs, as shown in Fig. 3. This assumption is reasonable because, firstly, the deflections are small, and secondly, if the boundary layer is close to separation, it will have minimal streamwise velocity near the reattachment point downstream of the flap, as seen in Fig. 3. This allows the mass flow into the plenum to be modeled as a consequence of the pressure difference across a gap, which increases proportionally in the streamwise direction. Figure 2a shows the actual situation and Fig. 2b shows the equivalent situation for theoretical modeling. Thus, L_G is the equivalent streamwise orifice width.

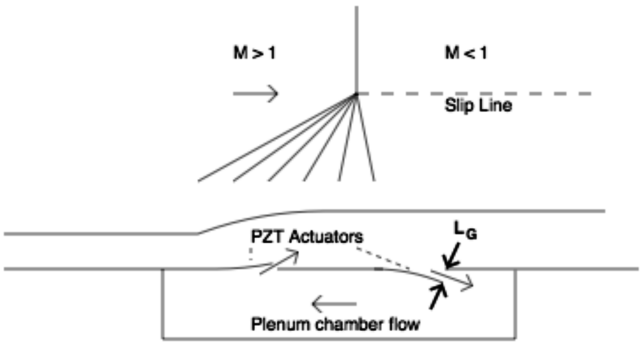

a) Flap control of shock wave/boundary layer interaction

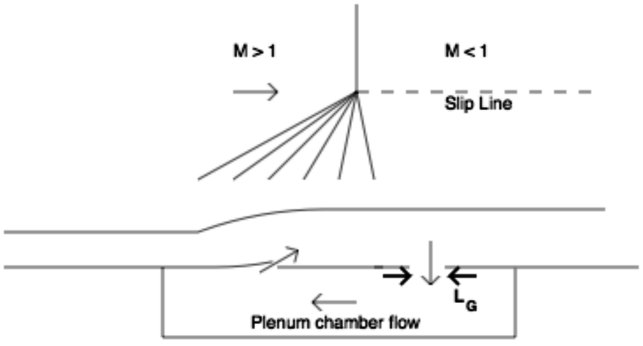

b) Flow model

Fig. 2 Flap control of shock wave/boundary-layer interaction: a) actual flap geometry: flaps deflected by bending up and down; b) flow model: upstream flap bends up, downstream flap opens horizontally.

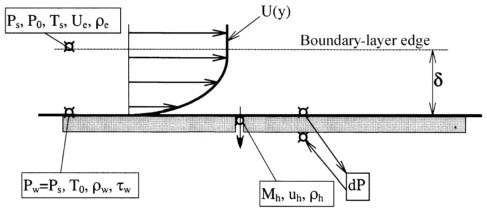

Fig. 3 Flow configuration and definitions [12].

B. Downstream Mass Flow Through a Single Orifice/Slot

The mass transfer (suction) across the downstream flap into the plenum is modeled based on the perforated plate analysis of Doerffer and Bohning [12], as illustrated in Fig. 3. In the figure, the subscripts s, o, e, w, and h denote the static, stagnation, edge, wall, and hole (slot) conditions, respectively. The pressure drop across a single hole/slot, irrespective of size, is given as (see Doerffer and Bohning [12])

$$\frac{dP}{P_o} = \left[\left(\frac{1}{1.2}\right)^{\frac{1}{0.55}} + b(BM_h)^{\frac{1}{a}}\right] M_h^{\frac{1}{0.55}} \tag{1}$$

where

$$B = \frac{\tau_w}{\rho_h u_h^2/2}$$

and $a = 1.52$, $b = 25$, $P_{oh} = P_s = P_2$, and $dP = (P_2 - P_1)/2$, and P_1 and P_2 are the static pressures upstream and downstream of the shock, respectively. The density, velocity, and Mach number are denoted by ρ, u, and M, respectively. The total temperature T_o is assumed constant throughout.

Various assumptions have been made in the preceding equation. First, it is assumed that the stagnation pressure at the entrance to the orifice P_{oh} is the same as the reservoir pressure for the flow in the orifice and is also equal to the downstream static pressure P_2. Another assumption is that the dynamic pressure above the orifice is not recovered, so that P_{oh} is the same as the downstream static pressure P_2. Further, because the Mach number in the cavity is small, this is also equal to the plenum chamber pressure. These assumptions have been justified through experimental data by Doerffer and Bohning [12] for a compressible flow through a perforated plate for adiabatic flows up to freestream Mach numbers $M \leq 2$. In the present instance, we apply this approach to an orifice/slot of unit width and show that this is quite reasonable a posteriori.

Again, following Doerffer and Bohning [12], when the tangential stream velocity is small, or if suction effects are taking place in a separated flow region, such as at an SBLI location as in the present instance, then we might set $\tau_w \approx 0$ in Eq. (1), so that

$$\frac{dP}{P_2} = M_h^{\frac{1}{0.55}}\left[\left(\frac{1}{1.2}\right)^{\frac{1}{0.55}}\right]$$

Rearranging gives

$$M_h = 1.2\left(\frac{dP}{P_2}\right)^{0.55} \approx \left[0.7\left(1 - \frac{P_1}{P_2}\right)\right]^{0.55} = f(M_1) \tag{2}$$

Here, M_h is the effective Mach number of the fluid across the orifice/slot. For a perforated plate with a large number of submillimetric holes, Doerffer and Bohning [12] give a limit for M_h of 0.57 based on the choking limit. If we relax this limit, because in the present case the slot is comparatively large, then the mass flow through the slot of unit width will be

$$\frac{m}{w} = L_G \frac{M_h}{(1 + \frac{\gamma-1}{2} M_h^2)^{\frac{\gamma+1}{2(\gamma-1)}}} P_2 \sqrt{\frac{\gamma}{RT_{w2}}}$$

where w is the span of the slot and L_G is the streamwise width of the slot, as in Fig. 2.

The width L_G can be further defined as (see [11])

$$L_G = \sqrt{\Delta_U^2 + (L_{GI} + \Delta L)^2}$$

This is calculated from the schematic represented in Fig. 2a and applied in Fig. 2b. L_{GI} is the initial gap at zero deflection and Δ_U is the flap deflection. Omission of the second term on the right-hand side of the preceding expression results in errors less than 0.5% for unimorph flap deflections up to 3 mm considered here. So, we can reasonably assume $L_G \approx \Delta_U$.

C. Upstream Flow Deflection Angles

The mass flow injected upstream of the shock is equal to the mass flow removed from downstream of the shock as a result of suction/bleed. This enables the calculation of the various angles as shown next.

Referring to Fig. 4, the total displacement growth angle θ_T may be taken to be the sum of the mass flow angle θ_m, unimorph flap deflection angle θ_U, and the angle θ_{δ^*}, due to the initial (upstream) uncontrolled displacement growth, so that

$$\theta_T = \theta_m + \theta_U + \theta_{\delta^*} \tag{3}$$

where $\theta_U = \Delta_U / L_U$ and the angle θ_m, due to the growth of the displacement thickness as a result of mass injection, is given by [11]

$$\sin\theta_m = \frac{m_{\text{inj}}}{m_{\text{total}}} \sin(180 - \theta_{\text{inj}}) \tag{4}$$

where m_{total} is the total mass of the displacement growth, m_{inj} is the injected mass flow, and θ_{inj} is the flow injection angle at the flap opening and assumed small so that $\cos\theta_{m_{\text{inj}}}$ is approximately unity in the following expression. The total mass m_{total} is given by [11]

$$m_{\text{total}} = \sqrt{m_{\text{inj}}^2 + m_{\delta^*}^2 + (2 m_{\text{inj}} m_{\delta^*} \cos\theta_{m_{\text{inj}}})} \tag{5}$$

The incoming mass within the displacement thickness δ^* is given by

$$m_{\delta^*} = \frac{7}{2} C_4 C_5^3 \left(\left\{ \frac{1}{12} \left[\frac{(\delta^*)^{2/7}}{C_5} \left(-\frac{4(\delta^*)^{4/7}}{C_5^2} - \frac{6(\delta^*)^{2/7}}{C_5} - 12 \right) \right] \right\} - \ell_n \left(1 - \frac{(\delta^*)^{2/7}}{C_5} \right) \right\} \right) \tag{6}$$

with

$$C_4 = \frac{2\rho_1 T_1 c_p \delta^{1/7}}{r U_1} \quad \text{and} \quad C_5 = \frac{2 T_{w1} c_p \delta^{2/7}}{r U_1^2}$$

where ρ, T, U, δ, δ^*, c_p, and r, are the density, static temperature, velocity, boundary-layer thickness, boundary-layer displacement thickness, specific heat at constant pressure, and temperature recovery factor, respectively. Subscripts 1 and w refer to upstream and wall conditions, respectively. These relations are based on the assumption that the wall is adiabatic and the boundary layer has a one-seventh power law profile. The detailed derivations of Eq. (6) and constants C_4 and C_5 are given in Couldrick [11].

The shock angle β of the leading leg of the lambda foot can then be determined iteratively using the standard oblique shock relation and the total displacement thickness growth angle θ_T as determined earlier:

$$\tan\theta_T = 2\cot\beta \left[\frac{M_1^2 \sin^2\beta - 1}{M_1^2(\gamma + \cos 2\beta) + 2} \right]$$

D. Triple Point Height

The triple point height h_{tp} is taken to be a combination of the flap deflection Δ_U, the boundary-layer thickness at the end of the flap δ_T, and the height δ_β, the vertical distance from the junction point of the leading leg of the lambda foot and the boundary-layer edge to the triple point. Figure 5 shows a schematic of the lambda structure model with definitions of various heights.

The downstream boundary-layer thickness δ_T is given by

$$\delta_T = \delta_o + L_U \tan\theta_\delta \tag{7}$$

where δ_o is the undisturbed boundary-layer thickness and θ_δ is the angle of the deflected boundary layer along the flap.

The triple point height δ_β is given by

$$\delta_\beta = L_\beta \tan\beta \tag{8}$$

where L_β is the sum of L_{inj}, the distance upstream of the main shock and the leading edge of the flap (see Fig. 6) and the distance of the upstream influence due to the flap deflection L_{inf}. There will also be an upstream influence due to injection per se, L_m, but for the small deflections involved, this can be ignored (Fig. 6). Then,

$$L_\beta \approx L_{\text{inj}} + L_{\text{inf}} \tag{9}$$

For a turbulent boundary layer, we can approximately put $L_{\text{inf}} \leq \delta_o$, so that

$$L_\beta \approx L_{\text{inj}} + \delta_o \tag{10}$$

Thus, from the knowledge of unimorph flap deflection and using Eqs. (7), (8), and (10), we can determine the triple point height h_{tp}. We are then in a position to apply these analytical predictions to both the MART system of [5] and the present piezoelectric unimorph flap actuators.

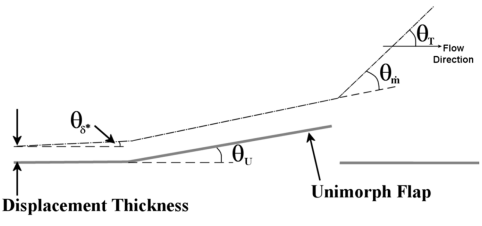

Fig. 4 Definition of flow deflection angles (not to scale).

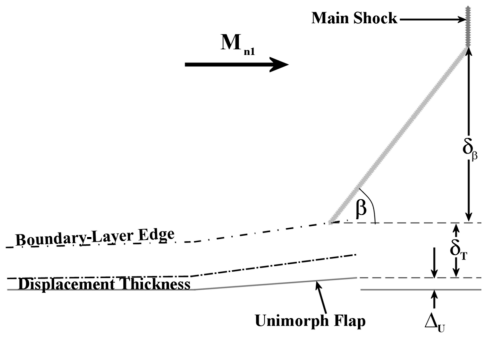

Fig. 5 Lambda structure model with definition of various heights.

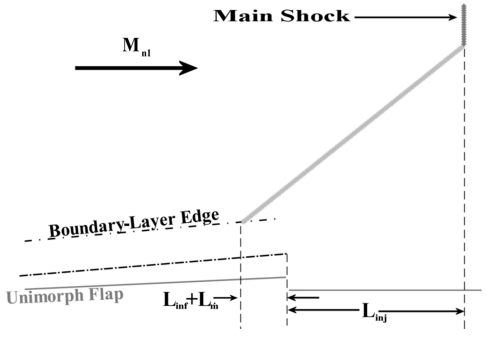

Fig. 6 Lambda structure model with definition of various lengths.

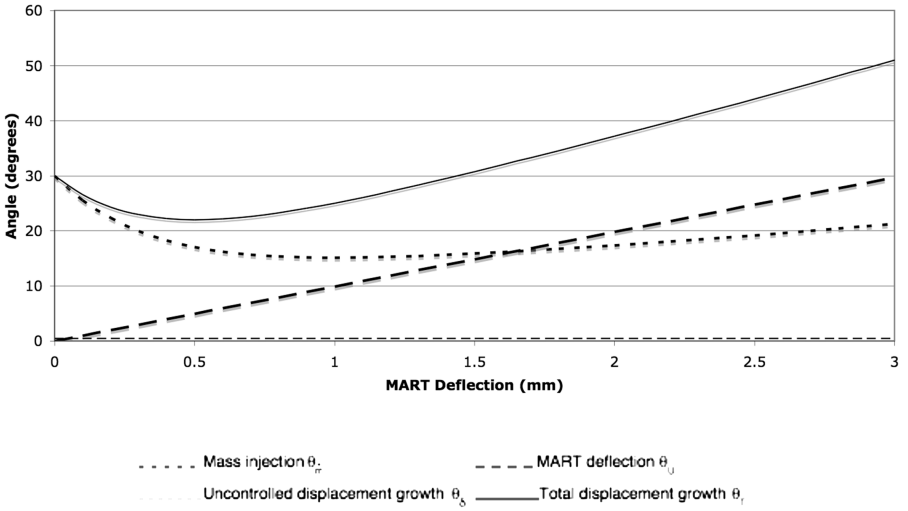

Fig. 7 Displacement thickness growth angle variation for the MART six-flap system.

III. Application to Mesoflaps for Aeroelastic Transpiration Control System

The system of mesoflaps for aeroelastic transpiration for SBLI control was developed by the research group at the University of Illinois at Urbana–Champaign, as mentioned earlier. The system consists of using six or four streamwise flap arrays, which are similar to the two-flap array configuration considered herein. The published MART control data of Hafenrichter et al. [5] are used to validate and test the analytical results derived earlier.

In the MART system considered in [5], the flow conditions were as follows: Mach number ahead of the normal shock $M_1 = 1.37$, reservoir pressure 210 kPa, undisturbed boundary-layer thickness $\delta_o = 2.6$ mm, displacement thickness $\delta_o^* = 0.36$ mm, and momentum thickness $\theta_o = 0.203$ mm. From the data in [5], the estimated plenum pressure was 35.8 kPa and the suction Mach number across the downstream flap and the plenum was 0.51.

A. Six-Flap system

Based on the preceding data, the various angles θ_m, θ_U, θ_{δ^*}, and θ_T, as described in Sec. II.C, were calculated and are shown in Fig. 7. It is seen that the mass injection effect initially reduces for deflections up to about 1 mm, after which it slowly increases at a nearly constant rate. It may also be noted that the total displacement thickness growth angle θ_T has a minimum at 23.5 deg corresponding to the flap deflection of about 0.5 mm ($1.39\delta_o^*$). In their experiments, Hafenrichter et al. [5] investigated three flaps of thicknesses 63.5, 101.9, and 150.6 μm, respectively, and concluded that the one with thickness 101.9 μm provided optimal control. They found that this corresponded to a deflection of approximately 0.484 mm. This agrees very well with the prediction of 0.5 mm deflection corresponding to a minimum total displacement growth angle (see Fig. 7) from the present analysis.

Hafenrichter et al. [5] found that, with thin flaps, the deflections were large, resulting in excess recirculation and sometimes causing fluttering of the flaps. On the other hand, thicker flaps with smaller deflections behaved more like conventional passive control with transverse injection and bleed. The optimum thickness resulted in a deflection that produced a nearly tangential injection and bleed as assumed in the present analysis. Figures 8a–8c are the shadowgraphs reproduced from Hafenrichter et al. [5]. It is noted that all the photographs show a series of leading oblique shocks forming the lambda structure. Considering Figure 8a first, the thinnest flap, the first shock has its origin at the junction of the flap array and the flat tunnel wall. The second shock that immediately follows it is due to the ramp effect caused by the flap deflection, and the third one is caused by the injection of the flow at the end of the flap. Figures 8b and 8c are largely similar except that, due to the increased thickness of the flaps, the deflections are small so that the first two shocks appear weaker as a result of reduced ramp effect. The third shock seems to have split into two, indicating flow injection effects in the transverse direction. This is particularly evident with the thicker (150.6 μm) flap. Also shown in these figures are the average angles of the third shock. These angles were directly measured from these photographs and hence are only approximate. They were not provided by the authors of [5].

From structural analysis [9,11], it was determined that with mesoflaps of thickness 63.5, 101.9, and 150.6 μm, the deflections produced were 2, 0.484, and 0.15 mm, respectively. Further, according to Hafenrichter et al. [5], the second flap following the first flap produces a deflection equal to half that of the first one. Thus, the

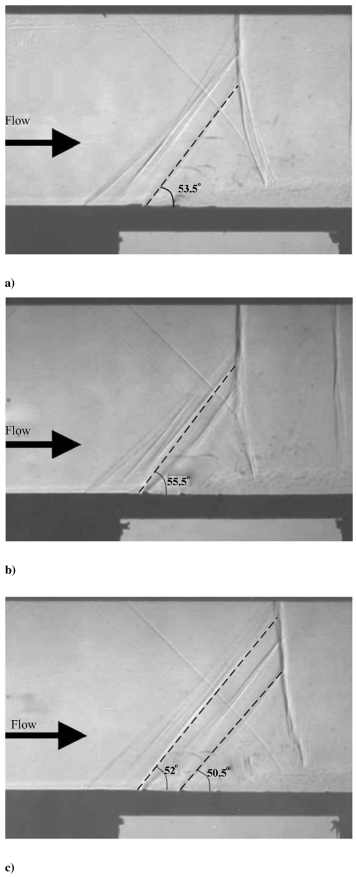

Fig. 8 Shadowgraph pictures of the MART six-flap system with mesoflap thicknesses of a) 63.5, b) 101.9, and c) 150.6 μm [5].

second flap following on from the first mesoflap of thickness 150.6 μm produces a deflection of 0.075 mm.

Using the preceding deflection information combined with the displacement thickness growth, we can then determine the oblique shock angle β of the leading leg of the lambda system using the analysis of Sec. II. The results are shown in Fig. 9. We note that, although the agreement with the 101.9 μm thickness flap is very good, the agreement with the flap thickness of 150.6 μm can be said to be only fair. In view of the various approximations and assumptions made in the analysis, this is considered reasonable. However, it is interesting to note that the optimum configuration with flap of thickness 101.9 μm, as determined in [5], lies on the theoretical curve, showing that, with this configuration, both the upstream injection and the downstream suction are nearly tangential as assumed in the analysis. It is also consistent with the deflection giving minimum displacement thickness growth angle (Fig. 7).

B. Four-Flap System

Performing a similar analysis on the four-flap system described in [5], we obtain the results shown in Fig. 10. We note that the minimum total displacement thickness angle $\theta_{T\min}$ for the four-flap system is 20.8 deg, corresponding to a flap deflection of 0.67 mm ($1.86\delta_o^*$). Structural analysis [9,11] of a mesoflap of thickness 190.5 μm used in [5] for the four-flap system suggests a thickness of 0.6 mm. Hafenrichter et al. [5] also found that the four-flap system of mesoflaps with thickness 190.5 μm provided a near optimal control of SBLI and was deemed better than the six-flap system. Figure 11

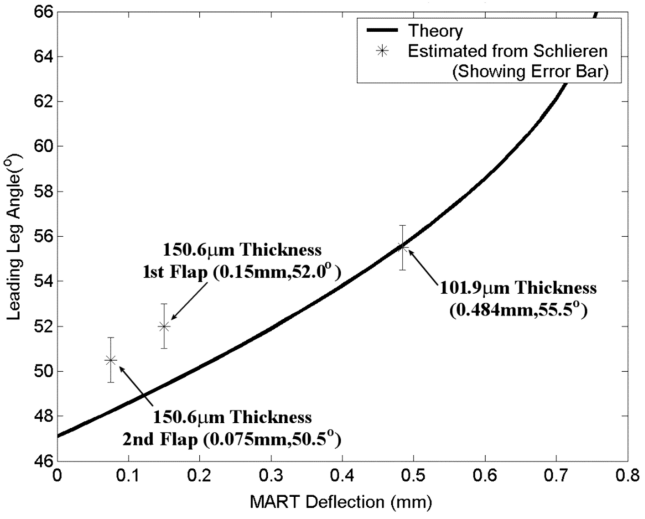

Fig. 9 The leading leg shock angle variation for mesoflap deflection of the MART six-flap system.

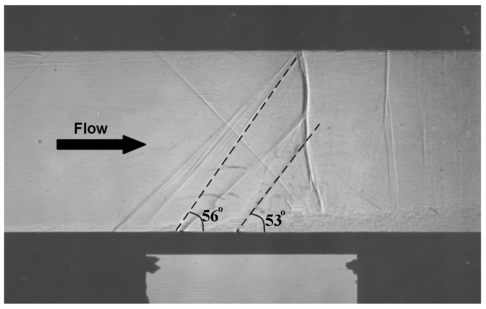

Fig. 11 Shadowgraphs of the MART four-flap system with a mesoflap thickness of 190.5 μm, [5].

shows the shadowgraph of the four-flap system with flaps of thickness 190.5 μm from [5]. The angles estimated by the present authors for the two leading and following flaps are also indicated on the photograph.

Figure 12 shows the theoretically estimated leading leg shock angle plotted against deflection and compared with the experimental results of Hafenrichter et al. [5]. Again, as in Fig. 9, agreement is reasonable, confirming the applicability of the analysis presented herein.

IV. Unimorph Flap System for Unswept Normal Shock Wave/Turbulent-Boundary-Layer Interaction at $M_1 = 1.5$

A. Experiments

Next, we describe experiments with a unimorph flap system for an unswept normal shock wave/boundary-layer interaction (UNSBLI) control at a Mach number of 1.5. These experiments were carried out in the transonic section of tunnel number 2 at the Engineering Department of the University of Cambridge, United Kingdom. Figure 13a shows the tunnel arrangement and the control region. The tunnel test section is 114 mm wide, 178 mm high, and the control plate on the floor is 172 mm in length. Manual control of the stagnation pressure, along with a second throat, allows the recovery shock to be positioned at $X = 0$, which is the start of the downstream unimorph flap position (Fig. 13b). The experiments made use of the interaction between the normal recovery shock and the naturally grown turbulent boundary layer on the tunnel floor. The undisturbed flow conditions for the interaction study were as follows: unit Reynolds number of $23.65 \cdot 10^6/\text{m}$, boundary-layer thickness $\delta_o = 7.54$ mm, and boundary-layer displacement thickness $\delta_o^* = 1.46$ mm. For a test section static pressure of 41 kPa, the flaps will then have approximately 30 kPa pressure difference acting across them. The plenum chamber, 38 mm in depth, is placed underneath the control plate in the floor of the test section. The plenum is covered by the control plate containing the flaps and numerous pressure ports,

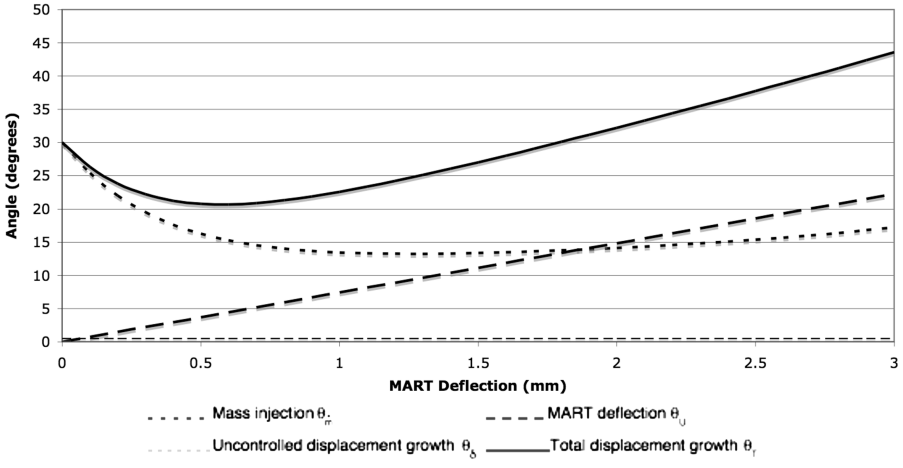

Fig. 10 Displacement thickness growth angle variation for the MART four-flap system.

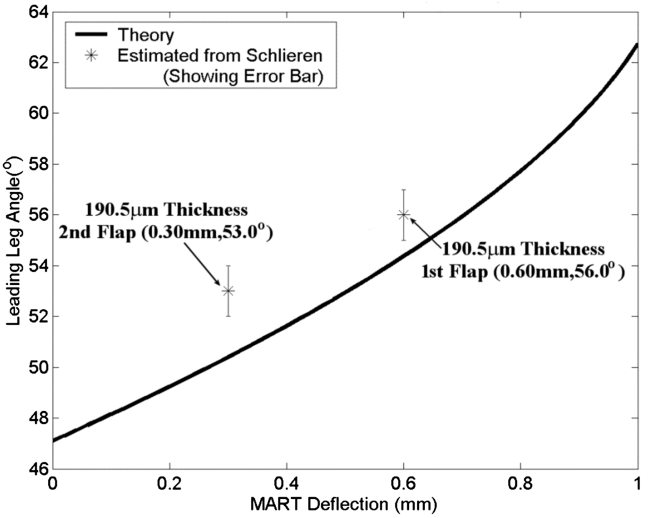

Fig. 12 The leading leg shock angle variation for mesoflap deflection for the MART four-flap system.

as shown in Fig. 13b. The flaps were cut into the plate by electrodischarge machining. The unimorphs, 1.77 mm total thickness, are made up of an aluminum substrate of thickness 1.25 mm, piezoelectric of thickness 0.5 mm, and a bond thickness of 0.02 mm, respectively. The unimorph tip deflection was shown to vary linearly with applied voltage. However, there is a limit to the deflection that can be achieved because of the possibility of piezoelectric material breakdown or depolarization. A limit of ±500 V had to be applied in the present investigation. This meant that only deflections of up to 0.35 mm were possible. Higher deflections were achieved by mechanical means. Full details of structural and electrical aspects of unimorphs and their design for the present application are given in [8]. The method of construction meant that there was a small gap of about 0.2 mm between the model skin and the flap. This in turn meant that the gap produced a continuous passive control of the SBLI along the two longitudinal edges and the front transverse edge of the flap. A piezoelectric ceramic is bonded to the underside of the flap and a voltage is applied to control the actuator deflection and hence the mass transfer rate.

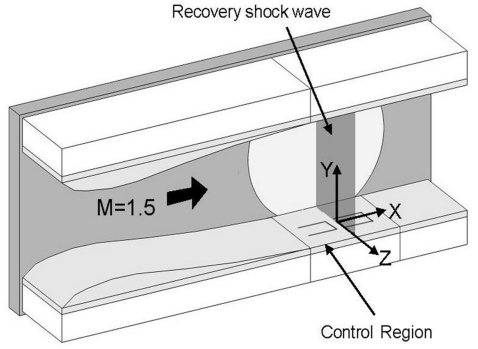

a)

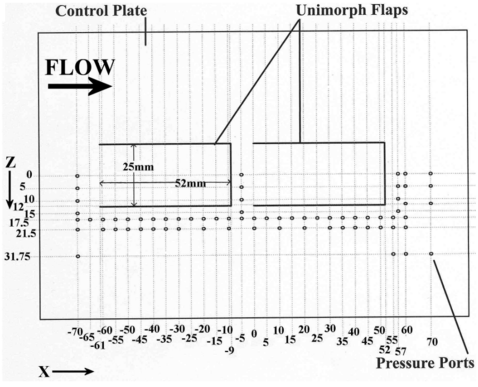

b)

Fig. 13 Schematic of the experiment showing a) wind-tunnel arrangement, and b) control plate details.

B. Results and Discussion

Figure 14 shows schlieren photographs with unimorph flap control in closed and open flap configuration. These were achieved with applied voltages of +500 and −500 V, respectively. It was found that, in the closed configuration shown in Fig. 14a (+500 V), the flap exhibited a deflection of 0.09 mm, which induced some mass transfer although nominally the deflection should be zero. The maximum deflection obtained with −500 V was 0.35 mm in the open configuration shown in Fig. 14b. In both photographs, the first oblique shock originates from the junction of the leading edge of the control plate and the upstream tunnel floor. The second oblique shock is due to the localized boundary-layer thickening as a result of fluid injection from the side slots formed by the gap between the flap and the control plate skin, referred to and discussed in Sec. IV.A. This is a localized effect and hence the shock appears weaker than the first oblique shock. The angle of this shock as well as the leading leg of the lambda shock are indicated on the photographs. Also indicated is the triple point height. Another point to note is that the second oblique shock angle in the flap open position (Fig. 14b) is slightly less than in the closed position (Fig. 14a). This is because, with flaps open, the main mass transfer occurs at the front of the flap so that spanwise effects are diminished.

The analysis of the unimorph system for a UNSBLI at an upstream Mach number of 1.5 can be done using the approach described in Sec. II and using the knowledge of undisturbed boundary-layer and displacement thickness characteristics as given in Sec. IV.A. The calculations were done for a pressure difference across the normal shock of 29.8 kPa and a suction Mach number M_h of 0.615. These predictions are shown in Fig. 15. We note that the mass injection effect θ_m initially decreases with an increase in deflection, showing asymptotic behavior as a result of balance between the

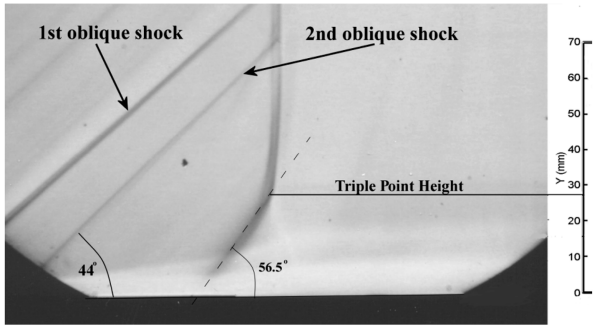

a)

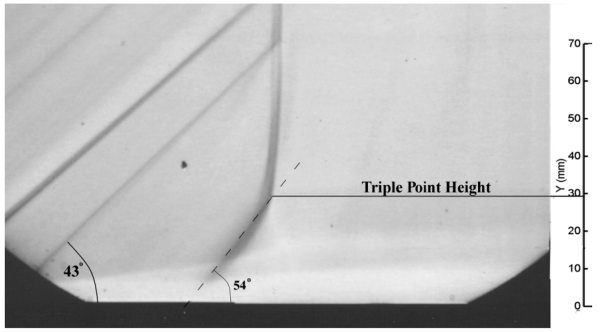

b)

Fig. 14 Schlieren pictures of the $M_1 = 1.5$ SBLI of unimorph flap control with a) 500 V (closed flaps) and b) −500 V (open flaps).

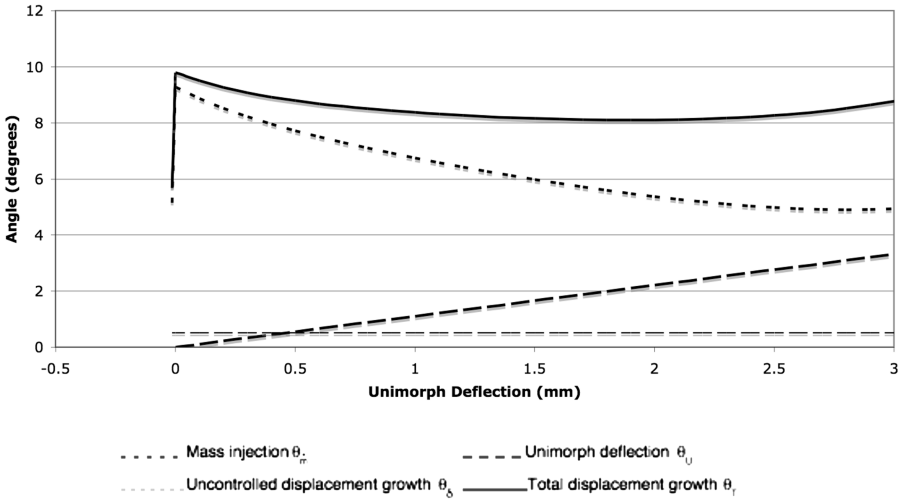

Fig. 15 Displacement thickness growth angle variation for unimorph flap deflection at $M_1 = 1.5$.

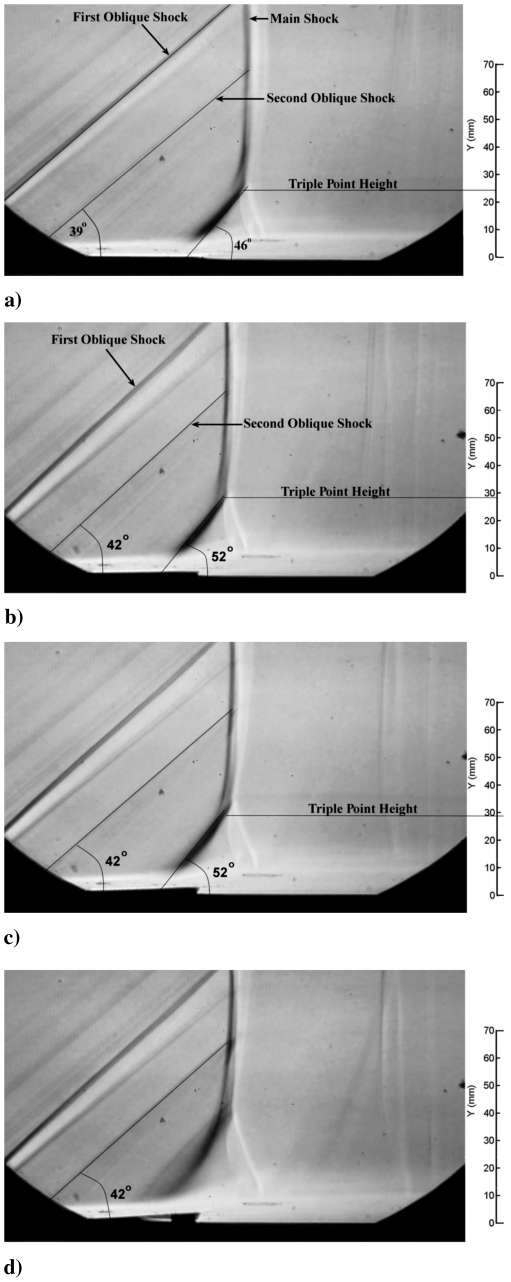

Fig. 16 Schlieren pictures of the $M_1 = 1.5$ UNSBLI with set unimorph flap deflections of a) 0, b) 1, c) 2, and d) 3 mm.

reduced injection angle and the increasing mass flow. The minimum total displacement thickness growth angle θ_T occurs for a deflection of 1.5 mm or approximately $1\delta_o^*$. This suggests that, for optimum performance, a deflection of about 1.5 mm is needed. However, as mentioned earlier, the unimorph actuators, when *actively* controlled, could only produce a maximum deflection of 0.35 mm at −500 V. The presently available piezoelectric materials are unable to produce greater strains (see Crawley [13]). A series of runs were therefore conducted at set flap deflections to evaluate the performance achievable and to predict the amount of deflection required for optimum control. A mechanical device allowed a continuous adjustment of the amount of deflection via a screw and pot system located in the plenum chamber. With this system, flap deflections of 0, 1, 2, and 3 mm, were studied. The 0 mm uncontrolled deflection was examined first to see if it would provide characteristics similar to the closed case under applied voltage when it was actively shut off.

Figures 16a–16d show schlieren photographs for set unimorph flap deflections of 0, 1, 2, and 3 mm, respectively. Again, the first oblique shock is the same as in Fig. 14. The inclination of the second oblique shock is slightly different because of different effects of boundary-layer thickening as a result of different flow deflections. Another feature to note is that the leading leg of the lambda structure of the normal bifurcated shock for the actively closed flap case and the nominally set zero deflection case are different. The reason for this, as pointed out earlier, is that, with the actively closed flap, there was still a gap of 0.09 mm, which resulted in some mass transfer

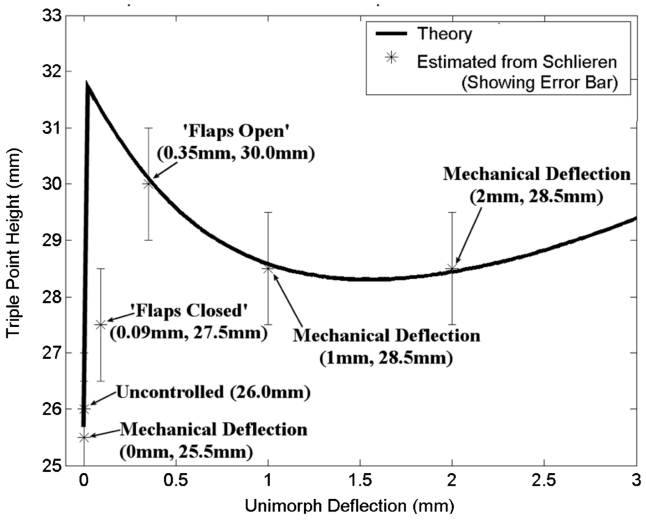

Fig. 17 Leading leg shock angle variation for unimorph deflection.

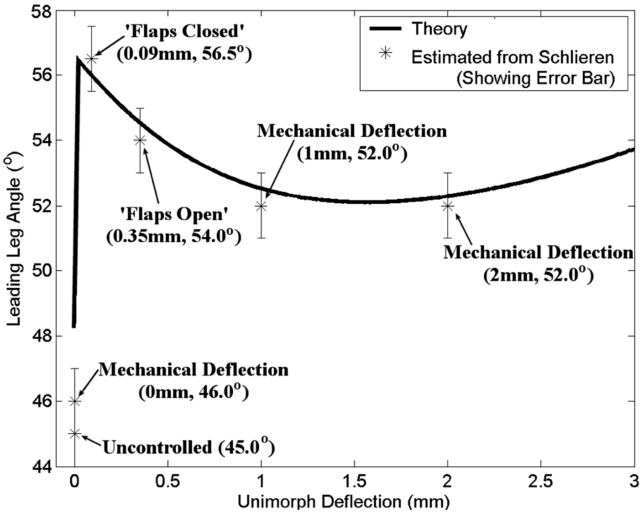

Fig. 18 Triple point height variation with unimorph deflection.

(leakage) giving an oblique shock angle of 56.5 deg in Fig. 14a instead of 46 deg as in Fig. 16a. The other features to be noted in Figs. 16a–16d are the triple point, its height, and the slipstream emanating from the triple point. It should be pointed out that the measured angles are necessarily approximate. Their accuracy has been estimated by taking four separate samples, including a maximum and minimum, and then applying a two-tail test with 90% confidence.

Figure 17 shows that the leading leg shock angles of the lambda foot of the bifurcated shock agree reasonably well with the theory. This is true with both actively controlled and mechanically set deflections. From Fig. 17, it is seen that, for optimum control, a unimorph deflection of 1.5 mm is required, giving the corresponding angle of the leading leg of the lambda foot as 52 deg. However, the experimental data suggest a deflection of 1 mm to generate this shock and angle. In view of the approximations in the measurement of deflections, this is considered reasonable.

Also shown in Fig. 17 is the uncontrolled case (solid wall) of UNSBLI with separation at a Mach number of 1.5, studied in the same facility by Holden [14], which showed an angle of 45 deg for the leading leg of the bifurcated lambda shock. The fact that the 0 mm case and the uncontrolled case produce nearly the same shock angle is again reassuring. The vertical solid line illustrates the mass transfer or leakage effect due to the 0.09 mm gap in the flap closed position.

Figure 18 shows the variation of the triple point height and there is a good agreement between the theoretical estimates and the measured values. Once again, it is seen that optimum deflection seems to be between 1 and 1.5 mm. Overall, the results from Figs. 16–18 show that there is a tradeoff between the total pressure and viscous losses for optimal deflection, within the limit of inhibiting boundary-layer separation.

V. Conclusions

A theoretical model is proposed to predict the effects of flap deflection on the displacement thickness growth angles, the leading angles of the bifurcated lambda shock, and the triple point height in an unswept normal shock wave/turbulent-boundary-layer interaction control. The analysis enables one to predict the optimum flap deflection required to control the UNSBLI and eliminate separation. Application of the theory to the MART system control, developed by the University of Illinois at Urbana–Champaign group, and to the present piezoelectric flap control system have both shown that the theory shows good agreement with experimental data. Briefly, the analysis has shown that deflections on the order of δ_o^* (the undisturbed displacement thickness) are required to control the interaction. With the MART systems, optimal control was achieved with deflections between $1.4\delta_o^*$ and $1.86\delta_o^*$ depending on the number of flap arrays. For the present unimorph piezoelectric two-flap system, the optimum deflection for control was $1\delta_o^*$. The optimal deflection for SBLI control is a tradeoff between reducing the total pressure losses, as implied by the increase in triple point height, and minimizing viscous losses.

Acknowledgments

The experimental investigation described in this paper was conducted in the Cambridge University Engineering Department as part of a collaboration program. The authors are very grateful to Holger Babinsky for his advice and to Harriet Holden for her help during the experiments. The work was supported by the Australian Research Council Linkage Program.

References

[1] Nagamatsu, H. T., Ficarra, R. V., and Dyer, R., "Supercritical Aerofoil Drag Reduction by Passive Control," AIAA Paper 1985-0207, 1985.

[2] Raghunathan, S., "Passive Control of Shock-Boundary Layer Interaction," *Progress in Aerospace Sciences*, Vol. 25, No. 3, 1988, pp. 271–296. doi:10.1016/0376-0421(88)90002-4

[3] Gibson, T. M., Babinsky, H., and Squire, L. C., "Passive Control of Shock Wave/Boundary Layer Interactions," *The Aeronautical Journal*, Vol. 104, No. 1033, 2000, pp. 129–140.

[4] Delery, J., and Bur, R., "Shock Wave/Boundary Layer Interaction and Control Techniques," Univ. of Southampton Press Paper 6010, July 1999.

[5] Hafenrichter, E. S., Lee, Y. L., Dutton, J. C., and Loth, E., "Normal Shock/Boundary Layer Interaction Control Using Aeroelastic Mesoflaps," *Journal of Propulsion and Power*, Vol. 19, No. 3, 2003, pp. 264–472.

[6] Wood, B., Loth, E., and Guebelle, P., "Mesoflaps for Aeroelastic Transpiration for SBLI Control," AIAA Paper 99-0614, 1999.

[7] Jaiman, R. K., Loth, E., and Dutton, J. C., "Simulations of Normal Shock Wave/Turbulent Boundary Layer Interaction Control Using Mesoflaps," AIAA Paper 2003-445, 2003.

[8] Couldrick, J. S., Gai, S., Milthorpe, J., and Shankar, K., "Normal Shock Wave/Turbulent Boundary Layer Interaction Control Using 'Smart' Piezoelectric Flap Actuators," *The Aeronautical Journal*, Vol. 109, No. 1101, 2005, pp. 577–583.

[9] Couldrick, J. S., Shankar, K., Gai, S., and Milthorpe, J., "Design of Smart Flap Actuators for Swept Shock Wave/Turbulent Boundary Layer Interaction Control," *Structural Engineering and Mechanics: An International Journal*, Vol. 16, No. 5, 2003, pp. 519–532. doi:10.1296/SEM2003.16.05.01

[10] Couldrick, J. S., Gai, S. L., Milthorpe, J. F., and Shankar, K., "Active Control of Swept Shock Wave/Turbulent Boundary Layer Interactions," *The Aeronautical Journal*, Vol. 108, No. 1080, 2004, pp. 93–101.

[11] Couldrick, J. S., "A Study of Swept and Unswept Normal Shock Wave/Turbulent Interaction and Control by Piezoelectric Flap Actuation," Ph.D. Thesis, Univ. of New South Wales, Canberra, Australia, 2006.

[12] Doerffer, P. P., and Bohning, R., "Modelling of Perforated Plate Aerodynamics Performance," *Aerospace Science and Technology*, Vol. 4, No. 8, 2000, pp. 525–534. doi:10.1016/S1270-9638(00)01063-4

[13] Crawley, E. F., "Intelligent Structures for Aerospace: A Technology Overview and Assessment," *AIAA Journal*, Vol. 32, No. 8, 1994, pp. 1689–1699. doi:10.2514/3.12161

[14] Holden, H. A., "Transonic Shock/Boundary Layer Interaction Control Using Three-Dimensional Devices," Ph.D. Thesis, Engineering Dept., Univ. of Cambridge, Cambridge, England, U.K., 2004.